Highlighting a research article from Prof. Guo-Bin Ding's laboratory at Institutes of Biomedical Sciences/School of Life Sciences, Inner Mongolia University, Hohhot, China.

Biosynthesized tumor acidity and MMP dual-responsive plant toxin gelonin for robust cancer therapy

Prof. Guo-Bin Ding's laboratory is working on tumor microenvironment-targeted delivery of macromolecular agents (proteins and nucleic acids). This article introduces a biosynthesized tumor acidity and MMP dual-responsive plant toxin gelonin (TPpG), TPpG could efficiently enter into and kill MMP-2 overexpressing HT1080 cells under weakly acidic condition, and notably inhibited subcutaneous HT1080 xenograft growth in mice.

As featured in:

See Guo-Bin Ding, Mingqiang Qiao, Zhuoyu Li *et al.*, *Biomater. Sci.*, 2024, **12**, 346.

rsc.li/biomaterials-science

PAPER

Check for updates

Biosynthesized tumor acidity and MMP dual-responsive plant toxin gelonin for robust cancer therapy†

Guo-Bin Ding, [ID] *‡[a,b] Huiyan Cao,‡[b] Chenchen Zhu,[b] Fangyuan Chen,[b] Jiaqi Ye,[a] Bin-Chun Li, [ID] [b] Peng Yang,[b] Roland H. Stauber, [ID] [b,c] Mingqiang Qiao*[b] and Zhuoyu Li [ID] *[b]

Among all kinds of anticancer agents, small molecule drugs produce an unsatisfactory therapeutic effect due to the lack of selectivity, notorious drug resistance and side effects. Therefore, researchers have begun to pay extensive attention to macromolecular drugs with high efficacy and specificity. As a plant toxin, gelonin exerts potent antitumor activity *via* inhibiting intracellular protein synthesis. However, gelonin lacks a translocation domain, and thus its poor cellular uptake leads to low outcomes of antitumor response. Here, tumor acidity and matrix metalloproteinase (MMP) dual-responsive functional gelonin (Trx-PVGLIG-pHLIP-gelonin, TPpG), composed of a thioredoxin (Trx) tag, a pH low insertion peptide (pHLIP), an MMP-responsive motif PVGLIG hexapeptide and gelonin, was innovatively proposed and biologically synthesized by a gene recombination technique. TPpG exhibited good thermal and serum stability, showed MMP responsiveness and could enter tumor cells under weakly acidic conditions, especially for MMP2-overexpressing HT1080 cells. Compared to low MMP2-expressing MCF-7 cells, TPpG displayed enhanced *in vitro* antitumor efficacy to HT1080 cells at pH 6.5 as determined by different methods. Likewise, TPpG was much more effective in triggering cell apoptosis and inhibiting protein synthesis in HT1080 cells than in MCF-7 cells. Intriguingly, with enhanced stability and pH/MMP dual responsiveness, TPpG notably inhibited subcutaneous HT1080 xenograft growth in mice and no noticeable off-target side effect was observed. This ingeniously designed strategy aims at providing new perspectives for the development of a smart platform that can intelligently respond to a tumor microenvironment for efficient protein delivery.

*a*Institutes of Biomedical Sciences/School of Life Sciences, Inner Mongolia University, Hohhot 010070, China. E-mail: ding@imu.edu.cn, dinggb2012@sxu.edu.cn
*b*Institute of Biotechnology, Key Laboratory of Chemical Biology and Molecular Engineering of Ministry of Education, Shanxi University, Taiyuan 030006, China. E-mail: qmq@sxu.edu.cn, lzy@sxu.edu.cn
*c*Nanobiomedicine Department/ENT, University Medical Center Mainz, Mainz 55131, Germany
†Electronic supplementary information (ESI) available. See DOI: https://doi.org/10.1039/d3bm01779f
‡Guo-Bin Ding and Huiyan Cao are the co-first authors of this work.

1. Introduction

Cancer causes millions of deaths annually and has gained utmost attention worldwide.[1,2] Among different cancer treatment options, small molecule-based traditional chemotherapy remains the mainstream choice but shows rather disappointing outcomes in patients because of the lack of selectivity, drug resistance and side effects.[3–5] Due to their unparalleled efficacy and unmatched specificity, macromolecular therapeutics hold great potential to overcome the limitations of small-molecule drugs and have attracted significant attention.[6–8] Over the past few decades, we have witnessed immense development of protein-based macromolecular agents and the field of protein therapeutics has expanded rapidly.[9–11] However, protein drugs generally show poor cellular internalization and low stability in systemic circulation due to their intrinsic hydrophilic nature,[12,13] which greatly compromises their therapeutic efficacy. Hence, a great number of delivery strategies were explored to improve the therapeutic effect of protein drugs.[13–16]

As a special family of cytotoxic polypeptides, ribosome-inactivating proteins (RIPs) exert anticancer activity by binding to large ribosomal subunits and irreversibly inhibiting protein synthesis.[17,18] Gelonin, a type I RIP with *N*-glycosidase enzymatic activity, shows unrivalled efficacy in killing cells by cleaving 28S rRNA.[19] However, it has been reported that gelonin significantly inhibits protein synthesis in cell-free systems but has little inhibitory effect on intact cells with plasma mem-

brane due to the lack of a cell membrane binding domain.[20] Construction of a fusion protein is a widely employed approach to combine the properties of different protein components and obtain a new protein with intriguing qualities.[21] Yang and Shin *et al.* designed a variety of fusion proteins using gelonin and membrane active peptides to enhance the cellular uptake and targeting ability of gelonin, such as TAT-gelonin,[22–24] gelonin-melittin,[25] F3-gelonin,[26] gelonin-anti-IGF-1R affibody[27] and gelonin-chlorotoxin.[28] Nonetheless, these fusion proteins either have no targeting ability or rely on affinity ligand-mediated active targeting, and the targeting efficiency is undermined by tumor heterogeneity. Therefore, there is an urgent requirement to develop a universal targeting strategy independent of specific biomarkers for efficient gelonin delivery.

Hypoxia, lack of nutrients and high rate of aerobic glycolysis produce a unique microenvironment of high lactate and low pH conditions within a solid tumor.[29] As an adaptive feature of most cancers, acidity is a metabolic hallmark at all stages of tumor progression and can be exploited for tumor diagnosis and targeted therapy.[30] pH low insertion peptide (pHLIP) is an acid-triggered, tumor-targeting peptide derived from bacteriorhodopsin C helix. It is unstructured at neutral pH and will insert its C-terminus across cell membranes *via* forming transmembrane α-helix under acidic conditions.[31] Conjugation of cell-impermeable molecules to the C-terminus of pHLIP will significantly facilitate their intracellular delivery. Importantly, the pHLIP-based delivery modality takes advantage of the acidic tumor environment, and it does not rely on the expression level of tumor-specific antigens.[32] Therefore, pHLIP can serve as a powerful vehicle for highly effective delivery of a broad range of theranostic cargoes including magnetite nanoparticles,[33,34] STING agonist,[35] peptide nucleic acids,[36–38] enhanced green fluorescent protein (EGFP)[39] and pleiotropic cytokine interleukin-2 (IL-2).[40] Recently, a double-switch pHLIP system has been developed for selective enrichment of circulating tumor microenvironment-derived extracellular vesicles (cTME-EVs).[41] Our group has previously used pHLIP to deliver an autophagy-inducing polypeptide,[42] an antitumor protein[43] and a siRNA-loaded nanovehicle.[44]

Matrix metalloproteinases (MMPs) are a family of zinc-dependent enzymes that are involved in tumor initiation, progression, and metastasis.[45] A large body of evidence demonstrated that many MMPs, particularly MMP-2 and MMP-9, are overexpressed and overactivated in most solid tumors, and therefore, they represent ideal cancer biomarkers and pharmacologic targets for cancer therapy.[45,46] In this work, we genetically engineered a functional gelonin fusion protein (denoted as Trx-PVGLIG-pHLIP-gelonin, TPpG) for the first time. As shown in Fig. 1a, TPpG is composed of four different fragments with divergent functions–a thioredoxin (Trx) tag, an MMP-2/9-cleavable peptide (PVGLIG), a pHLIP with a sequence of AAEQNPIYWARYADWLFTTPLLLLDLALLVDADEGT and plant toxin gelonin. The Trx tag could enhance the solubility and stability of fusion proteins, the PVGLIG motif is responsive to MMP-2/9 and can be cleaved in a tumor

microenvironment,[47,48] pHLIP can endow the fusion protein with tumor acidity-targeting ability, and gelonin is an antitumor plant toxin. After reaching tumor tissues, the Trx tag in TPpG will be cleaved by the overexpressed MMP-2/9 to generate pG (pHLIP-gelonin), and the display of pHLIP on the surface of pG will markedly favor cell membrane permeation of gelonin under an acidic tumor microenvironment and then effectively inhibit protein synthesis and trigger cell death (Fig. 1a). The purified TPpG was comprehensively characterized, and its thermal and serum stabilities were assessed. The cellular internalization and *in vitro* antitumor efficacy of TPpG were examined in MMP2-overexpressing HT1080 cells and low MMP2-expressing MCF-7 cells. Furthermore, we explored the apoptosis-induction activity of TPpG and analyzed its inhibitory effect on intracellular protein synthesis. Thereafter, the *in vivo* antitumor activity and biosafety of TPpG were evaluated in mouse models bearing xenograft fibrosarcoma HT1080 tumors by intravenous administration.

2. Materials and methods

2.1. Materials

An anti-His-tag primary antibody was purchased from Yeasen Biotechnology (Shanghai) Co., Ltd. A hypersensitive ECL chemiluminescence kit was provided by Sevenbio (Beijing, China). Sulforhodamine B (SRB), 4′,6-diamidino-2-phenylindole (DAPI) and crystal violet were obtained from Beijing Solarbio Science & Technology Co., Ltd. A carboxyfluorescein diacetate succinimidyl ester (CFDA-SE) cell proliferation detection kit was purchased from the Beyotime Institute of Biotechnology (China). 3-(4,5-Dimethylthiazol-2-yl)-2,5-diphenyltetrazolium bromide (MTT) was provided by Gentihold (Beijing). An Annexin V/PI double-staining apoptosis assay kit and a caspase-3 activity assay kit were obtained from BestBio (Shanghai, China). Primary antibodies against Ki-67 and caspase-3 were provided by Beijing Bioss Biotechnology Co., Ltd (China).

2.2. Expression and characterization of Trx-PVGLIG-pHLIP-gelonin (TPpG)

The expression vector pET32a-*PVGLIG-pHLIP-gelonin* was obtained by whole-plasmid PCR using the pET32a-*pHLIP-gelonin* plasmid as a template. The recombinant plasmid pET32a-*PVGLIG-pHLIP-gelonin* was transformed into competent *E. coli* BL21 (DE3) (Beijing TransGen Biotech, China) and incubated at 37 °C. When the optical density (OD) at 600 nm reached 0.6–0.8, isopropylthiogalactoside (IPTG) (final concentration: 0.5 mM) was added, and the culture was incubated overnight (16 °C, 180 rpm). The cells were then collected by centrifugation, resuspended in phosphate buffer (PB, 300 mM NaCl, 20 mM imidazole, pH 7.0) and lysed by sonication. The cell lysate was centrifuged at 13 000 rpm for 30 min, and the supernatant was loaded onto Ni-nitrilotriacetic acid (NTA) resin (Suzhou Biodragon Immunotechnologies Co., Ltd, China), washed with 20 mM Tris (80 mM imidazole, 150 mM NaCl, pH 8.0), and eluted with 20 mM Tris (200 mM imidazole,
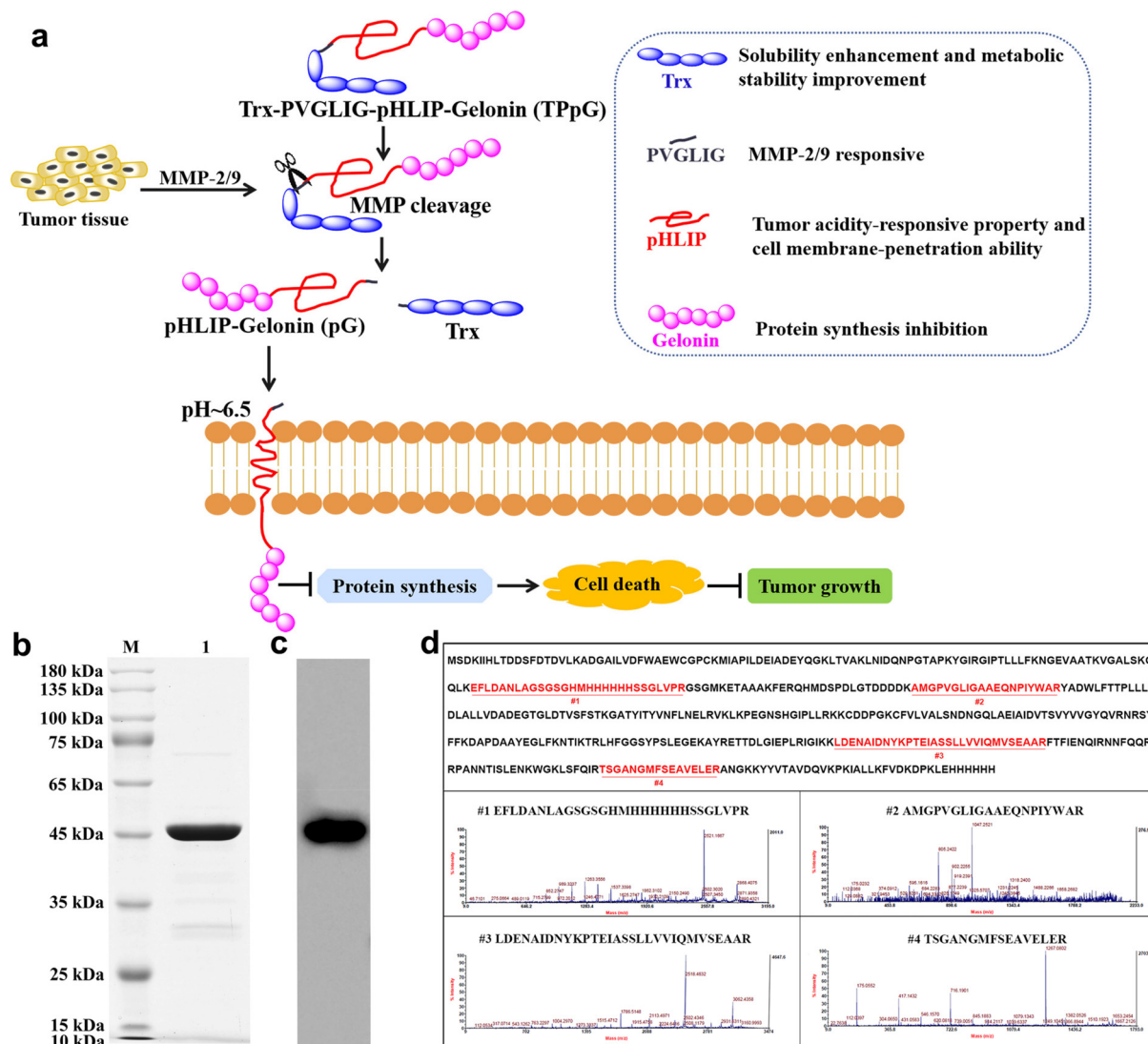
Fig. 1 Schematic illustration of the structural composition, mechanism of action and characterization of functional gelonin fusion protein (TPpG). (a) TPpG contains four fragments with different properties, and it could specifically accumulate in tumors, be cleaved by the upregulated MMP-2/9 to generate pG (pHLIP-gelonin). pG will efficiently deliver gelonin to tumor cells *via* formation of transmembrane α-helix under weakly acidic conditions (pH 6.5) and results in tumor growth inhibition by inhibiting protein synthesis and triggering cell death. (b) SDS-PAGE of purified TPpG. Lane M is a protein molecular weight marker, and lane 1 is purified TPpG. (c) Detection of purified TPpG using an anti-His antibody by western blotting. (d) Mass spectrometry analysis of the TPpG band excised from the SDS-PAGE gel, showing the existence of four representative peptide fragments (#1−4) after proteolysis that conform to the theoretical amino acid sequence of TPpG (shown in red color).

150 mM NaCl, pH 8.0). The obtained TPpG solution was desalted and concentrated by ultrafiltration, and the purified TPpG was subjected to sodium dodecyl sulphate polyacrylamide gel electrophoresis (SDS-PAGE) and western blot analysis. Densitometry analysis was performed with ImageJ software to analyze the purity of TPpG, and the production yield was determined by BCA assay. After SDS-PAGE, the TPpG band was cut out and subjected to MALDI-TOF-MS analysis conducted by Sangon Biotech Co., Ltd (Shanghai, China). The recombinant gelonin was obtained according to our previous report[19] and used as the control in this study. To evaluate its MMP-responsiveness, TPpG was incubated with activated collagenase IV for 2 h and was analyzed by 12% SDS-PAGE.

2.3. Thermal and serum stability of TPpG

The thermal stability of TPpG was analyzed using a Chirascan circular dichroism (CD) spectrometer (Applied Photophysics, UK). CD spectra of purified TPpG (4 μM) in the range of 195–260 nm were recorded at different temperatures (30, 35, 40, 45, 50, 55, 60, 65, 70, 75, 80, 85, 90, and 95 °C) at a heating rate of 2 °C min^{-1}, and the scanning speed was 1 nm s^{-1}. For the serum stability test, TPpG (10 μM) was incubated with either a neutral (pH 7.4) or acidic (pH 6.5) fresh DMEM containing 10% fetal bovine serum (FBS) at 37 °C for different time periods (0, 1, 2, 4, 6, 12, 24 and 48 h). TPpG samples collected at different times were mixed with a loading buffer and

subjected to SDS-PAGE, and the band intensity was quantified with ImageJ software. The TPpG band intensity at 0 h was set as 100%.

2.4. Cellular uptake of TPpG

Gelonin and TPpG were labeled with fluorescein isothiocyanate (FITC) to produce FITC-gelonin and FITC-TPpG, which is favorable for the cellular internalization study. A human fibrosarcoma cell line (HT1080) and a human breast cancer cell line (MCF-7) were seeded into 12-well plates with coverslips and incubated overnight. Cells were treated with 1 μM FITC-gelonin or FITC-TPpG at pH 7.4 or 6.5 for 6 h and washed three times with PBS. Cells were visualized by confocal laser scanning microscopy (CLSM) after the nuclei were stained with DAPI. For western blot analysis, HT1080 and MCF-7 cells were seeded into 6-well plates and exposed to 1 μM gelonin or TPpG at pH 7.4 or 6.5 for 6 h. Cells were washed, harvested and lysed. Intracellular protein was collected and subjected to SDS-PAGE, and intracellular gelonin or TPpG was determined by western blotting using an anti-His antibody. The relative level of TPpG or gelonin was quantified by ImageJ software and normalized to the control group. The expression level of GAPDH was used as an internal reference.

2.5. MTT cell viability assay

HT1080 and MCF-7 cells were inoculated in 96-well plates and incubated overnight. Then different concentrations (0, 0.001, 0.01, 0.1, 1 and 10 μM) of gelonin or TPpG were added and co-incubated at pH 7.4 or 6.5 for 48 h. The culture medium was replaced with a fresh serum-free medium (100 μL) and MTT (20 μL, 5 mg mL^{-1}). After incubation for another 4 h, the MTT solution was removed, dimethyl sulfoxide (150 μL) was added to each well, and the cell viability was analyzed by absorbance at 570 nm using a microplate reader.

2.6. Crystal violet staining assay

HT1080 and MCF-7 cells were seeded into 96-well plates and incubated for 24 h. Cells were exposed to different concentrations (0, 0.01, 0.1 and 1 μM) of gelonin or TPpG at pH 7.4 or 6.5 for 48 h. After removal of the medium, a crystal violet staining solution (0.5%) was added to each well and incubated for 20 min. Cells were washed three times with PBS and the cell images were recorded. To quantify the cell viability, 200 μL of methanol was added to each well and incubated for 20 min at room temperature, and then the absorbance at 570 nm was recorded.

2.7. CFDA-SE cell proliferation assay

HT1080 and MCF-7 cells were digested and stained with CFDA-SE. CFDA-SE labeled cells were seeded into 6-well plates, incubated for 24 h and treated with 1 μM gelonin or TPpG for 24 h at pH 7.4 or 6.5. After that, cells were harvested, washed twice with PBS, and filtered using a nylon mesh and the CFDA-SE intensity was analyzed by flow cytometry.

2.8. Sulforhodamine B colorimetric assay

Sulforhodamine B (SRB) colorimetric assay was performed according to the procedures in a previous report.[49] Briefly, HT1080 and MCF-7 cells were seeded into 96-well plates and incubated overnight. The cell medium was replaced with a fresh medium (pH 7.4 or 6.5) containing different concentrations (0, 0.1, 1, and 10 μM) of gelonin or TPpG and incubated for 48 h. Trichloroacetic acid (TCA) (100 μL, 10%) was added to each well and incubated at 4 °C for 1 h, and then the mixed solution was aspirated. After rinsing with water and air-drying, SRB solution (100 μL, 0.057%) was added, and the cell plate was allowed to stand at room temperature for 2 h, followed by rinsing with 1% acetic acid and air-drying. Ultimately, 200 μL of 10 mM Tris base solution (pH = 10.5) was added into each well and incubated in a shaker for 10 min, and the absorbance at 510 nm was measured using a microplate reader to quantify cell viability.

2.9. Cell apoptosis study

HT1080 and MCF-7 cells were seeded into 6-well plates and incubated for 24 h. After addition of 1 μM gelonin or TPpG, the cells were cultured for 48 h at pH 7.4 or 6.5. Then the cells were collected, washed twice with PBS and stained with Annexin V-FITC and propidium iodide (PI) successively. Finally, the cells were redispersed in 400 μL of binding buffer and filtered through a nylon mesh and the apoptotic cell ratio was determined by flow cytometry.

For caspase-3 activity measurement, HT1080 and MCF-7 cells were exposed to 1 μM gelonin or TPpG at pH 7.4 or 6.5, respectively, for 48 h. Cells were harvested and lysed, and the caspase-3 activity was determined using the caspase-3 activity assay kit (Beyotime, China) according to the manufacturer's protocol. The absorbance at 405 nm was recorded using a microplate reader and the relative caspase-3 activity was calculated.

2.10. Intracellular protein synthesis inhibition assay

HT1080 and MCF-7 cells were seeded into 6-well plates and incubated for 24 h. After exposure to 1 μM gelonin or TPpG at pH 7.4 or 6.5 for 48 h, the cells were washed three times with cold PBS and lysed with 1% Triton X-100. Cell lysates were harvested and centrifuged at 12 000 rpm for 30 min. Then the total protein content in the supernatant was measured using an enhanced BCA protein assay kit (Beyotime, China). The relative cellular protein levels were calculated, and the untreated group was used as the control.

2.11. Animal model and *in vivo* antitumor study

Four-week old female BALB/c nude mice were purchased from Beijing Vital River Experimental Animal Technology Co. Ltd (Beijing, China) and raised under specific pathogen-free (SPF) grade conditions. All animal experimental procedures were approved by the Animal Care and Use Committee of Inner Mongolia University (Hohhot, China). All animal experiments were performed in compliance with the guidelines set by

national regulations for the care and use of laboratory animals. To establish an HT1080 xenograft mouse model, 5×10^6 HT1080 cells in 100 μL of saline were subcutaneously injected into the armpits of its right anterior limbs. The tumor size was determined with a digital caliper and calculated using the equation: V (mm^3) = tumor length × (tumor width)^2/2. When the tumor grew to about 120 mm^3 (set as day 0), the HT1080 tumor-bearing mice were randomly divided into three groups (n = 5): saline, gelonin, and TPpG, and injected intravenously on days 0, 3, 6, and 9 with a dose of 0.35 μmol kg^{-1} of gelonin and TPpG and 5 mL kg^{-1} of saline. The tumor volume and body weight were recorded every 2 days for a period of 20 days. The relative tumor volume was normalized as V/V_0 (V_0 is the average tumor volume on day 0).

On day 20, all mice were sacrificed, and all tumors were collected and fixed in 4% paraformaldehyde. The paraffin-embedded tumors were sectioned and stained with hematoxylin and eosin (H&E), and the histological changes in tumor tissues were observed using an inverted microscope. An immunohistochemical study was carried out to detect the expression levels of Ki-67 and caspase-3 in tumor tissues using specific antibodies against Ki-67 and caspase-3, respectively. Furthermore, the apoptotic cells in tumor sections were determined by terminal deoxynucleotide transferase (TdT)-mediated dUTP nick-end labeling (TUNEL). The apoptotic cells displayed green fluorescence, while the cell nuclei were stained with DAPI and exhibited blue fluorescence.

2.12. *In vivo* biosafety assessment

Major normal tissues (heart, liver, spleen, lungs and kidneys) in each group were excised at day 20 and subjected to H&E staining. Histological examinations of these major organs were conducted to assess the *in vivo* biosafety of TPpG.

2.13. Statistical analysis

Data were shown as the mean ± standard deviation. Statistical analysis was performed using Student's t-test, $P < 0.05$ was considered to be significant, and $P < 0.01$ and $P < 0.001$ were considered highly significant.

3. Results and discussion

3.1. Biosynthesis and characterization of TPpG

The recombinant plasmid pET32a-*PVGLIG-pHLIP-gelonin* was successfully constructed, as confirmed by agarose gel electrophoresis (Fig. S1†). The recombinant plasmid was transformed into *E. coli* BL21 (DE3), with the expression of TPpG induced by addition of 0.5 mM IPTG, and incubated at 16 °C overnight. As shown in Fig. S2,† a strong band between 45 and 65 kDa was observed in lanes 2 and 4, while a relatively weak band at this position was detected in lane 3, indicating that TPpG was mainly expressed in the form of inclusion body and a small portion was in the soluble form. Then the supernatant fraction was purified by Ni-NTA affinity chromatography, only an intense band between 45 and 65 kDa can be seen in lane 1 of

Fig. 1b after purification, and the average purity of TPpG reached 95.13% as determined by densitometry analysis of the SDS-PAGE gels. A BCA protein assay kit confirmed that the average yield of TPpG was 0.898 mg L^{-1}. Furthermore, the successful biosynthesis of His-tagged TPpG was validated by western blot analysis using an anti-His antibody (Fig. 1c). The molecular weight of TPpG is 51 348 Da as analyzed by matrix-assisted laser desorption ionization time-of-flight mass spectrometry (MALDI-TOF-MS), consistent with the theoretical value (51 160 Da). The TPpG band was digested into peptides for mass spectrometry analysis, and 13 independent peptide fragments matched well with the TPpG sequence (Table S1†). Secondary mass spectrometry analysis of four representative peptide fragments (#1–4) from TPpG is shown in Fig. 1d. These results demonstrated that TPpG was biologically synthesized by prokaryotic expression and successfully purified by metal affinity chromatography.

Two well-known hallmarks of the tumor microenvironment are weak acidity (pH ∼6.5–7.1) and overexpression of matrix metalloproteinase-2 (MMP-2) in the extracellular matrix.[50] Next, the MMP-responsive property of TPpG was verified by SDS-PAGE after incubation with activated collagenase IV for 2 h. Interestingly, it can be seen clearly from Fig. S3† that two bands appeared at about 33 kDa and 17 kDa after incubation with collagenase IV for 2 h, confirming that TPpG could be cleaved by MMP and could produce two peptide fragments with molecular weights conforming to Trx and pHLIP-gelonin (pG).

3.2. Thermal and serum stability of TPpG

It has been reported that the integration of the thioredoxin (Trx) tag can improve the stability of the fusion protein.[51] First, the secondary structure of TPpG was determined by circular dichroism (CD) at 25 °C (Fig. 2a). CDNN (version 2.1) software indicated that TPpG contains 33.3% α-helix, 17.5% β-sheet, 16.7% β-turn and 33.0% random coil, and α-helix and random coil are the major secondary structure types of TPpG. Then the thermal stability of TPpG was evaluated by collecting the CD spectra in the range of 195–260 nm at different temperatures (30–95 °C). As shown in Fig. 2b, the CD spectra almost overlapped from 30 °C to 60 °C, while an obvious variation in the CD spectra was observed when the temperature reached 65 °C, suggesting that TPpG had good thermal stability and could retain its secondary structure below 65 °C. The T_m (melting temperature) value of TPpG is 62.0 °C as calculated by Global 3 software.

After administration *via* intravenous injection, the exposure of therapeutic proteins to body fluids (such as blood) may affect their stability and efficacy profile.[52] So to test its serum stability, TPpG was incubated with a 10% FBS-containing neutral (pH 7.4) or acidic (pH 6.5) cell medium at 37 °C for different time periods and subjected to SDS-PAGE analysis. A clear TPpG band as indicated by the red arrow could be observed in all lanes after incubation in the serum-containing medium of both pHs even after 48 h (Fig. 2c and e). The TPpG band was quantitatively analyzed by ImageJ software, and the
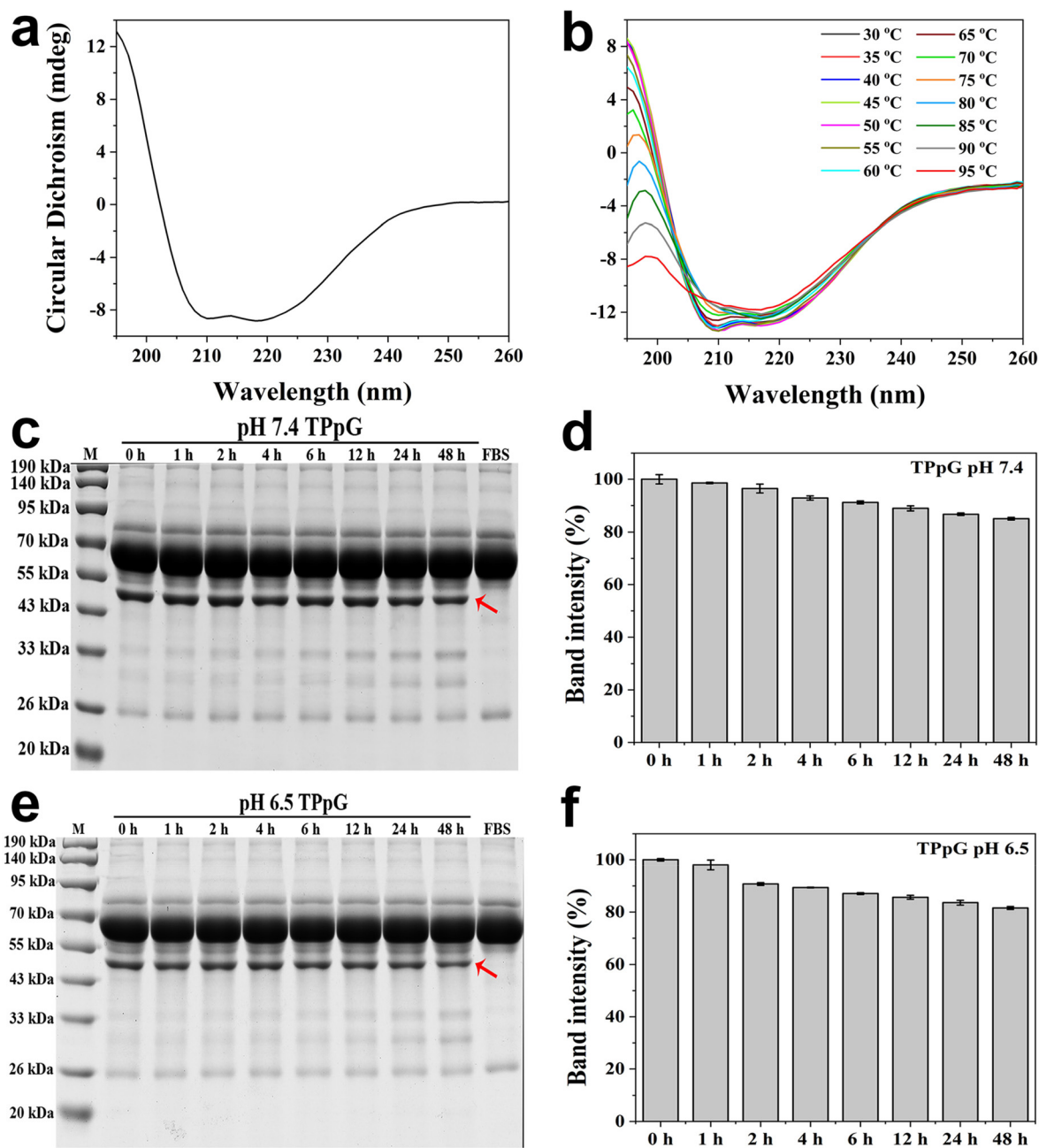
Fig. 2 Analysis of the thermal and serum stability of TPpG. (a) CD spectrum of TPpG (4 μM) at 25 °C and (b) CD spectra of TPpG (4 μM) at different temperatures (30–95 °C) collected using the circular dichroism spectrometer (Chirascan). (c and e) SDS-PAGE of TPpG (10 μM) after incubation with a neutral (pH 7.4) or acidic (pH 6.5) 10% FBS-containing cell medium at 37 °C for different time periods. Lane M is a protein marker, and the red arrows indicate the protein bands of TPpG. (d and f) Quantitative analysis of the TpG band intensity in c and e *via* ImageJ software. TPpG band intensity at 0 h was set as 100%.

protein band intensity was higher than 80% after 48 h of incubation in a neutral or acidic medium (Fig. 2d and f), indicating that TPpG displayed good serum stability and was suitable for anticancer applications.

3.3. Cellular uptake behavior of TPpG

Direct entry into the cytosol is required for the vast majority of intracellular applications of proteins.[53] To facilitate qualitative

and quantitative analysis of intracellular uptake, TPpG was labeled with fluorescein isothiocyanate (FITC), and the appearance of a strong absorption peak at 495 nm indicated the successful synthesis of FITC-TPpG (Fig. S4†). It has been reported that MMP2 is overexpressed in HT1080 cells and there is a low MMP2 level in MCF-7 cells;[54] thus, these two cell lines were employed for the cellular uptake study and gelonin was used as the control.

Gelonin showed poor cellular internalization in MCF-7 and HT1080 cells at both pHs, so only weak green fluorescence was observed (Fig. 3a and b). Likewise, TPpG was not able to enter into both cell lines efficiently under neutral conditions, and the intracellular green fluorescence was very weak. In contrast, the green fluorescence of both cells was significantly enhanced in the TPpG-treated group at pH 6.5, and the green fluorescence intensity was much stronger in HT1080 cells than in MCF-7 cells (Fig. 3a and b). Furthermore, the cellular uptake

of TPpG was evaluated by western blotting. As displayed in Fig. 3c and e, the gelonin band was slightly enhanced after gelonin treatment under neutral and acidic conditions in both cell lines. Similarly, there was also an increase in TPpG band intensity of varying degrees after TPpG treatment at pH 7.4. As expected, the TPpG band was markedly augmented in TPpG-treated MCF-7 and HT1080 cells under acidic conditions (Fig. 3c and e). Quantitative analysis demonstrated that the TPpG band intensity was 2.96-fold the control in HT1080 cells
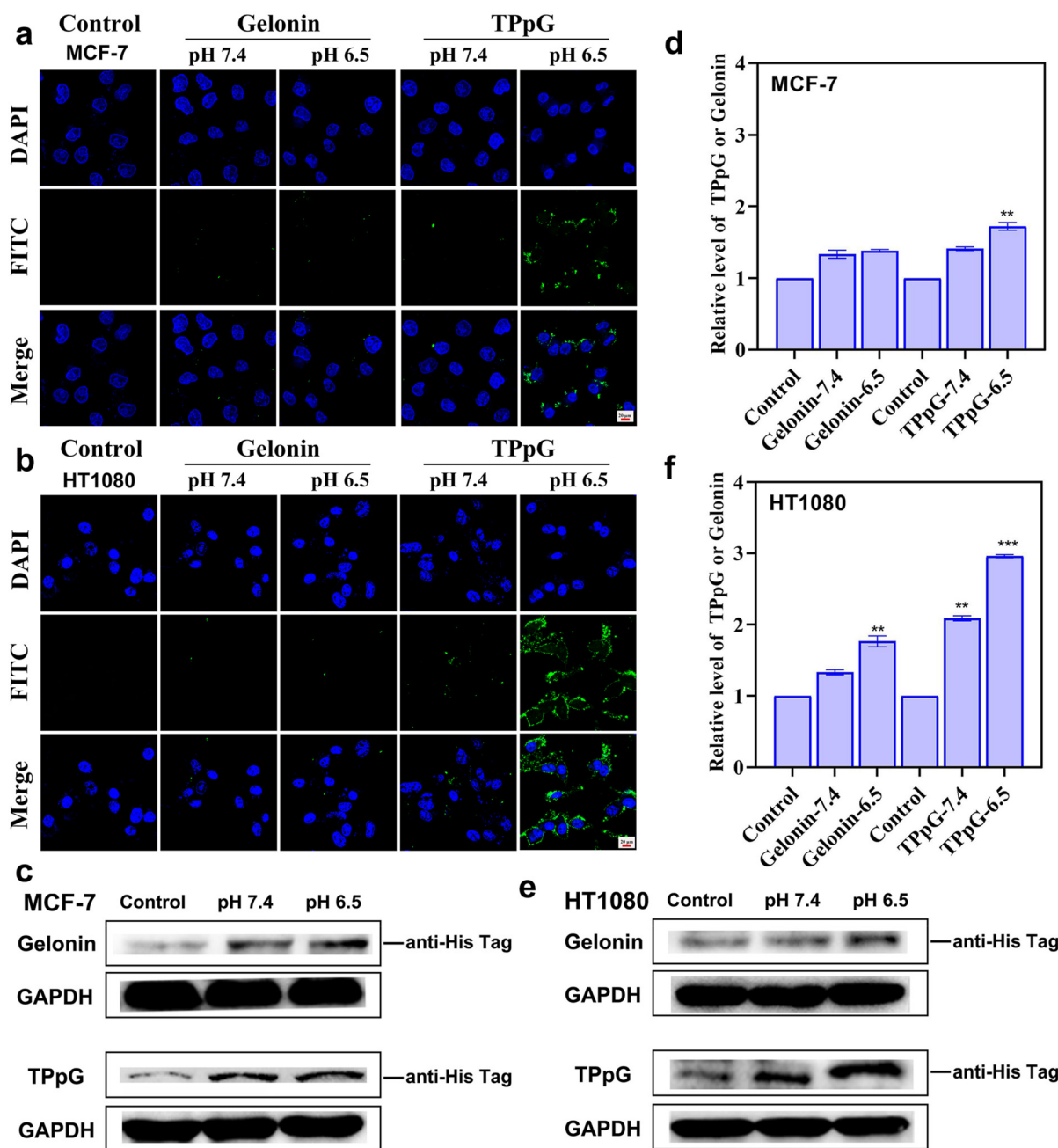

Fig. 3 Cellular uptake evaluation of TPpG in MCF-7 and HT1080 cells. CLSM images of MCF-7 (a) and HT1080 (b) cells after incubation with 1 µM gelonin or TPpG for 6 h at pH 7.4 or 6.5. Western blotting analysis of cellular uptake of gelonin or TPpG by MCF-7 (c) and HT1080 (e) cells using an anti-His antibody after incubation with 1 µM gelonin or TPpG for 6 h at two pHs (7.4 or 6.5). (d and f) Quantitative results of (c) and (e), respectively.

at pH 6.5 (Fig. 3f). The above results testify that gelonin itself can hardly enter into tumor cells at both pHs (7.4 and 6.5), TPpG displayed the pH/MMP dual-responsive ability, and it could effectively translocate gelonin into MMP2-overexpressing HT1080 cells under acidic conditions.

3.4. In vitro antitumor activity of TPpG

Benefitting from the pH/MMP dual-responsiveness of TPpG, massive gelonin molecules could be delivered to HT1080 cells

effectively under weakly acidic conditions. Thus the in vitro antitumor activity of TPpG was comprehensively investigated. First, an MTT assay was conducted to assess the cytotoxicity of TPpG. As shown in Fig. S5,† the inhibitory effect of gelonin on both cell lines is weak under neutral and acidic conditions, and the cell survival rate was still higher than 64% even at the highest concentration (10 μM), which is attributed to its poor intracellular uptake. Similarly, TPpG showed low cytotoxicity to MCF-7 cells with low MMP2 expression at the two pHs.
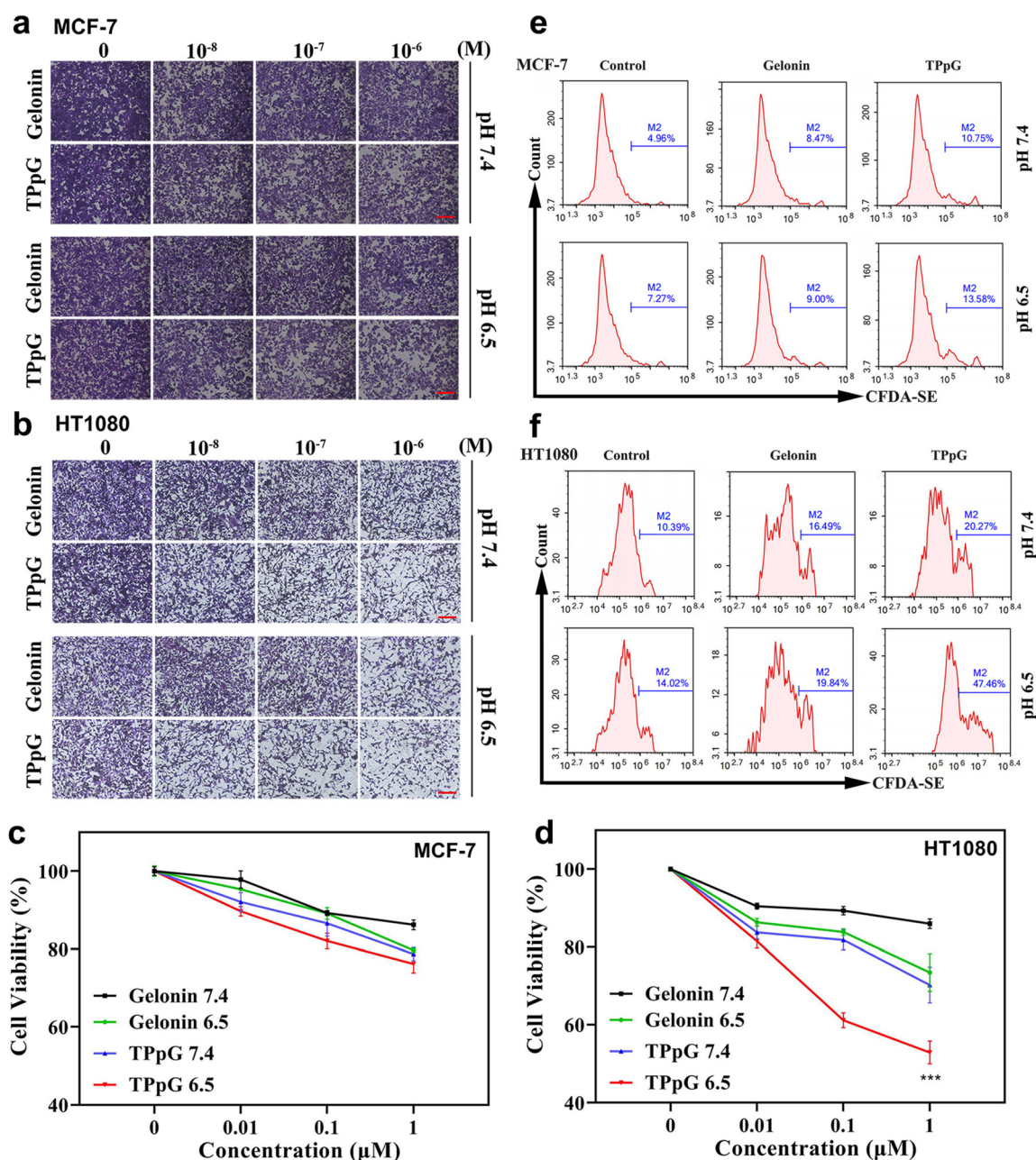
Fig. 4 In vitro antitumor activity of TPpG. (a–d) Crystal violet staining assay for examining the cell viability of MCF-7 (a and c) and HT1080 (b and d) cells after treatment with gelonin and TPpG of different concentrations (0, 0.01, 0.1 and 1 μM) for 48 h under neutral or weakly acidic conditions. (a and b) Representative images of MCF-7 and HT1080 cells after different treatments. The scale bars are 200 μm. (c and d) Quantitative results of (a) and (b), respectively. (e and f) Cell proliferation was analyzed by CFDA-SE staining assay. CFDA-SE labeled MCF-7 (e) and HT1080 cells (f) were incubated with 1 μM gelonin or TPpG for 24 h at two different pHs (7.4 and 6.5), and the CFDA-SE positive cell ratio was analyzed by flow cytometry.

The cell viability was 60.80% after treatment with 10 µM TPpG at pH 6.5 (Fig. S5b†), indicating that the presence of the Trx tag may affect the transmembrane activity of pHLIP. It is worth mentioning that TPpG exhibited pH-dependent cytotoxicity against HT1080 cells with high MMP2 expression (Fig. S5c and d†). After exposure to 10 µM TPpG for 48 h, the inhibitory rate reached 61.19% and 77.53% at pH 7.4 and 6.5, respectively. The IC$_{50}$ values of gelonin and TPpG against MCF-7 and HT1080 cells at two pHs were calculated according to the MTT data and are summarized in Table S2.† TPpG showed much lower IC$_{50}$ values than gelonin in the two tested cell lines and at the two pHs. The lowest IC$_{50}$ value was observed in TPpG-treated HT1080 cells at pH 6.5 (5.20 µM).

Subsequently, crystal violet staining was employed to examine the antitumor activity of TPpG. Gelonin exposure resulted in a slight decrease in cell density of the two cell lines at both pHs (Fig. 4a and b), and the cell survival rate was higher than 72% at a dose of 1 µM (Fig. 4c and d). The cytotoxicity of TPpG to MCF-7 cells was also relatively low at the two pHs, and no obvious change in cell number was observed (Fig. 4a and c). In comparison, TPpG exhibited dose and pH-dependent cytotoxicity against HT1080 cells, and the cell viability was lower than 51% at a concentration of 1 µM under acidic conditions (Fig. 4b and d).

To further validate the inhibitory effect of TPpG on the proliferation of the two cell lines, a CFDA-SE staining assay was utilized to assess the effect of TPpG on cell division. CFDA-SE is a cell membrane permeable fluorescent dye, and the equal distribution of CFDA-SE molecules to daughter cells after each cell division leads to a sequential halving of the fluorescence.[55]

Thus, an increase in cell division frequency is accompanied by a decrease in fluorescence intensity. As shown in Fig. 4e, in MCF-7 cells, the proportions of CFDA-SE positive cells in the gelonin-treated group were 8.47% and 9.00% at pH 7.4 and 6.5, respectively, slightly higher than those in the control group (4.96% and 7.27%) but lower than those in the TPpG group (10.75% and 13.58%). Interestingly, the anti-division activity of TPpG was significantly enhanced in HT1080 cells particularly under weakly acidic conditions with a CFDA-SE positive ratio of 47.46% (Fig. 4f), which was much higher than those of the control (14.02%) and gelonin-treated groups (19.84%). The above results indicated that the highly expressed MMP2 in HT1080 cells could cleave the PVGLIG sequence in TPpG, and the exposure of pHLIP was favorable for its transmembrane activity. Consequently, more gelonin molecules can be translocated into HT1080 cells under acidic conditions, contributing to the improved antitumor activity of TPpG.

3.5. Sulforhodamine B colorimetric assay

Sulforhodamine B (SRB) assay is one of the most commonly used approaches for *in vitro* cytotoxicity testing, which depends on the binding ability of SRB to cellular protein that has been fixed by trichloroacetic acid (TCA).[49] Therefore, the cytotoxicity of TPpG was further determined by SRB assay. As shown in Fig. 5, consistent with the MTT results, gelonin exerted low cytotoxicity to MCF-7 and HT1080 cells at both pHs, and the cell viability was higher than 64% even at the highest concentration (10 µM). TPpG also presented relatively weak inhibitory activity towards MCF-7 cells, with a cell viability of 60.40% at a dose of 10 µM under acidic conditions
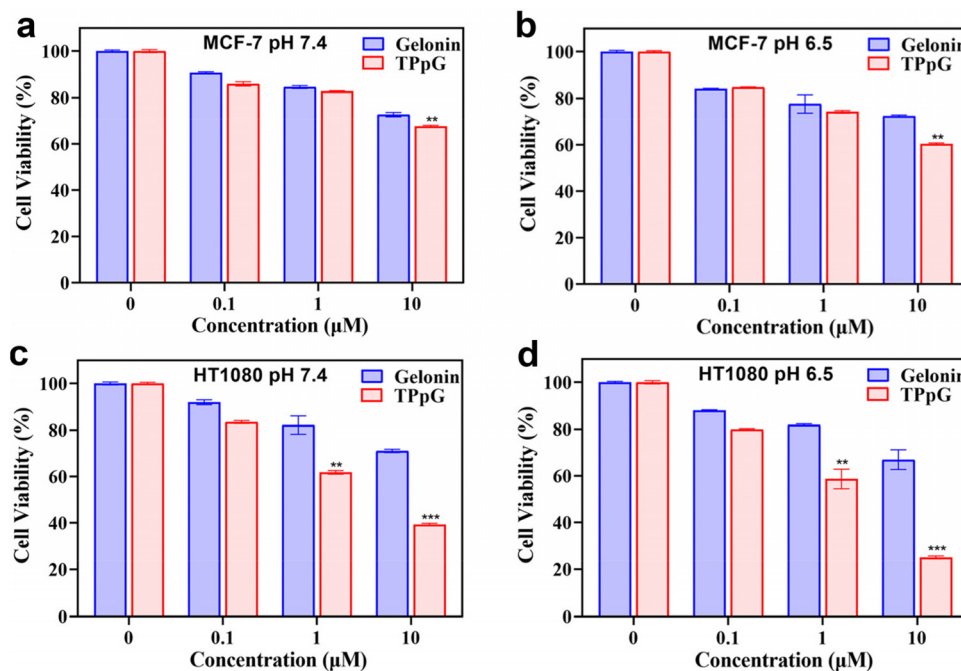

Fig. 5 Analysis of TPpG cytotoxicity against MCF-7 (a and b) and HT1080 (c and d) cell lines under neutral (a and c) or acidic (b and d) conditions using the SRB assay. MCF-7 cells and HT1080 cells were incubated with different concentrations of gelonin or TPpG at pH 7.4 or 6.5 for 48 h, and the cell viability was determined using the SRB method. ** indicates $P < 0.01$ and *** indicates $P < 0.001$ as compared to the control.

(Fig. 5b). Of note, pH and dose-dependent cytotoxicity was observed in TPpG-treated HT1080 cells, and the cell viabilities at pH 7.4 and 6.5 were 39.28% and 24.89% respectively after exposure to 10 μM TPpG for 48 h (Fig. 5c and d). Combined with the above results, we speculated that the Trx tag might hinder the transmembrane activity of TPpG, thereby impairing its antitumor activity.

3.6. TPpG induces apoptosis and suppresses intracellular protein synthesis

It has been reported that ribosome-inactivating proteins (RIPs) possess the capability of inducing cell apoptosis.[15] Subsequently, the apoptosis-induction ability of TPpG was assessed using an Annexin V-FITC/PI double-staining apoptosis assay kit and a caspase-3 activity assay kit. The results in Fig. 6a and b show that the apoptosis ratios were comparable under neutral and acidic conditions in the gelonin-treated group, which are 10.04% and 11.57% in MCF-7 cells and 19.91% and 23.87% in HT1080 cells. The proportion of apoptotic MCF-7 cells incubated with TPpG at pH 6.5 (22.79%) was slightly higher than that at pH 7.4 (19.82%) (Fig. 6a). Intriguingly, the apoptotic cell ratio of the TPpG-treated group was conspicuously increased to 64.05% in HT1080 cells at pH 6.5, which was significantly higher than that under neutral conditions (42.54%) (Fig. 6b). In parallel, caspase-3 activity assays were conducted in MCF-7 and HT1080 cells under the
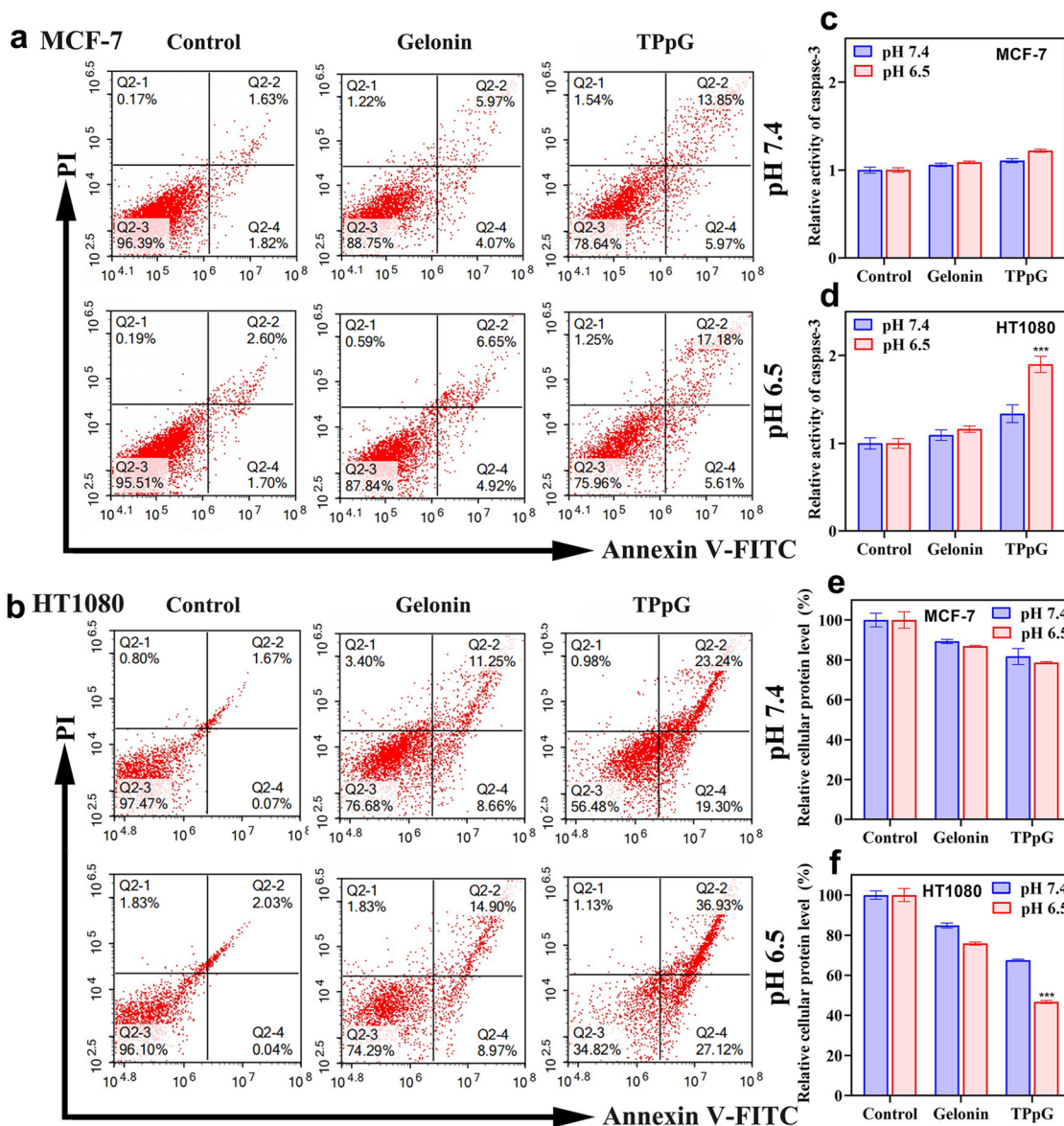
Fig. 6 *In vitro* apoptosis and intracellular protein level evaluation. MCF-7 and HT1080 cells were incubated with 1 μM gelonin or TPpG at pH 7.4 or 6.5 for 48 h. (a and b) Apoptosis in MCF-7 and HT1080 cells was analyzed by flow cytometry using the Annexin V-FITC/PI double-staining apoptosis assay kit. (c and d) The relative caspase-3 activity in MCF-7 and HT1080 cells was measured using the caspase-3 activity assay kit. (e and f) Intracellular protein level in MCF-7 and HT1080 cells was determined using the BCA protein assay kit. *** indicates $P < 0.001$ as compared to the control.

same conditions. Gelonin treatment led to a negligible increase in the caspase-3 activity in both cell lines (Fig. 6c and d), while TPpG caused a significant increase (1.89-fold the control) in the caspase-3 activity in HT1080 cells at pH 6.5 (Fig. 6d). In addition, in order to verify whether the *N*-glycosidase activity of gelonin was preserved in TPpG, the intracellular protein content was measured. As displayed in Fig. 6e and f, there was a decrease in the relative cellular protein level after gelonin treatment in both cell lines at the two pHs, and the relative cellular protein level

was higher than 75%. TPpG exhibited a weak inhibitory effect on protein synthesis in MCF-7 cells at the two pHs conditions, with relative protein levels of 81.65% and 78.58% at pH 7.4 and 6.5, respectively. Extraordinarily, TPpG markedly inhibited protein synthesis in HT1080 cells at pH 6.5 with a relative cellular protein level of 46.58% (Fig. 6f). These results revealed that TPpG could induce apoptosis and inhibit protein synthesis more effectively in MMP2-overexpressing HT1080 cells under weakly acidic conditions.
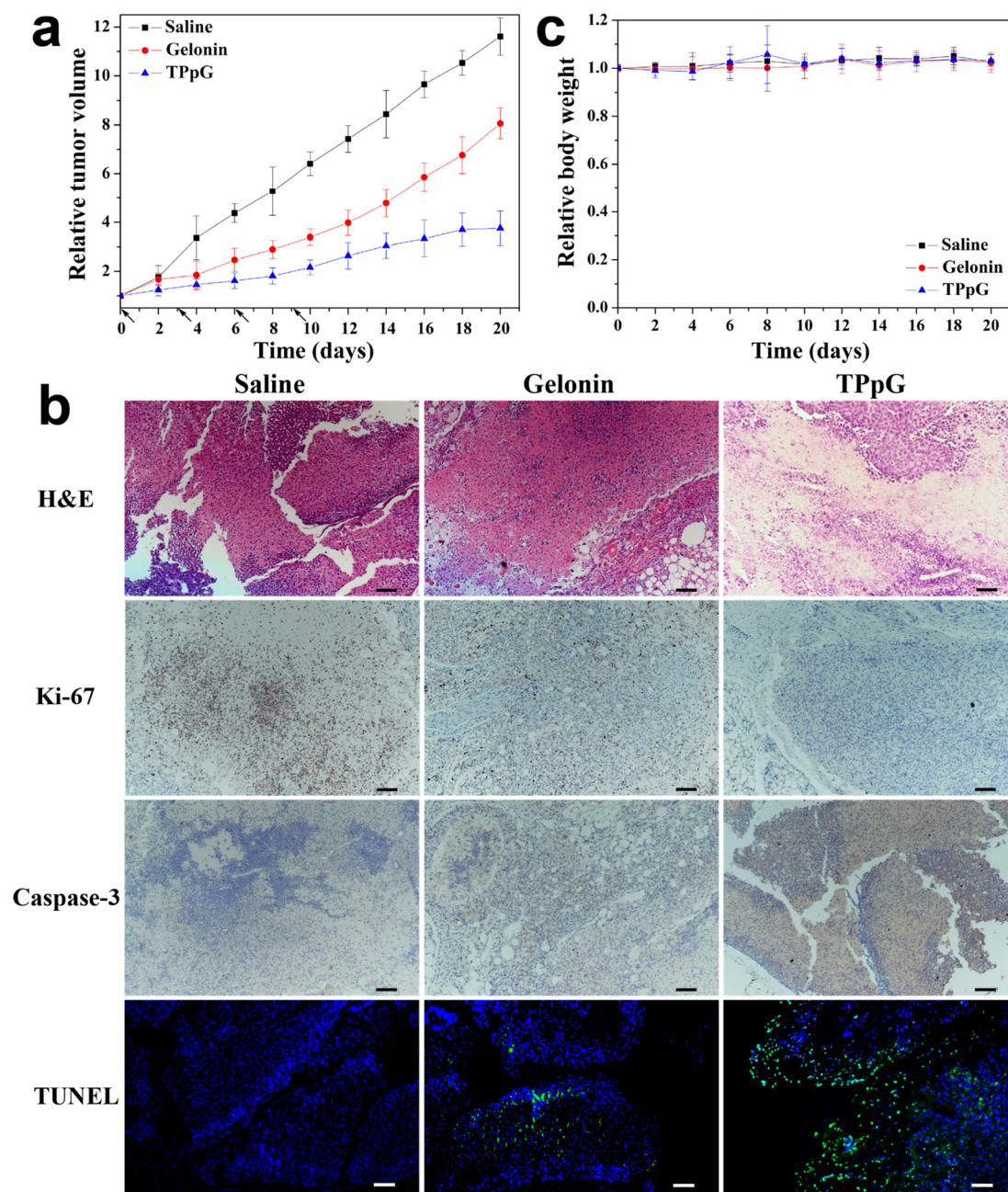

Fig. 7 *In vivo* antitumor activity of TPpG evaluated in a subcutaneous HT1080 tumor model. TPpG was administered *via* intravenous injection on day 0, 3, 6 and 9. (a) Relative tumor volume growth curves of different treatment groups (saline, gelonin and TPpG). The arrows indicate the administration time. (b) H&E staining, immunohistochemical staining (for detection of Ki-67 and caspase-3) and TUNEL assay of tumor tissues from different groups on day 20. The scale bars are 100 μm. (c) Relative body weight changes of mice after different treatments during the 20 days.

3.7. *In vivo* therapeutic performance and biosafety of TPpG

Inspired by the excellent *in vitro* antitumor activity of TPpG against MMP2-overexpressing HT1080 cells, the *in vivo* antitumor efficacy of TPpG and gelonin was evaluated in nude mice bearing subcutaneous HT1080 tumors. After four times of intravenous injection on days 0, 3, 6 and 9, the relative tumor volume and body weight of mice were monitored for 20 days. It could be seen from Fig. 7a that tumors in the saline group grew quickly and uncontrollably with a relative tumor volume of 11.61, and gelonin had limited anticancer activity (the relative tumor volume was 8.06) due to the poor cellular uptake and lack of targeting ability. As expected, the most suppressive ability against HT1080 xenografts was observed in the TPpG-treated group with a relative volume of 3.75, which was much more potent than that of the gelonin group (Fig. 7a). From the H&E staining results in Fig. 7b and Fig. S6,† we noticed that tumor cells in the saline group were well-organized and tightly arranged with an intact structure, while numerous apoptotic and dead cells were observed in tumor tissues after treatment with gelonin. Notably, TPpG treatment led to extensive damage in tumor tissues, characterized by the lowest cell density and the highest level of karyorrhexis (Fig. 7b).
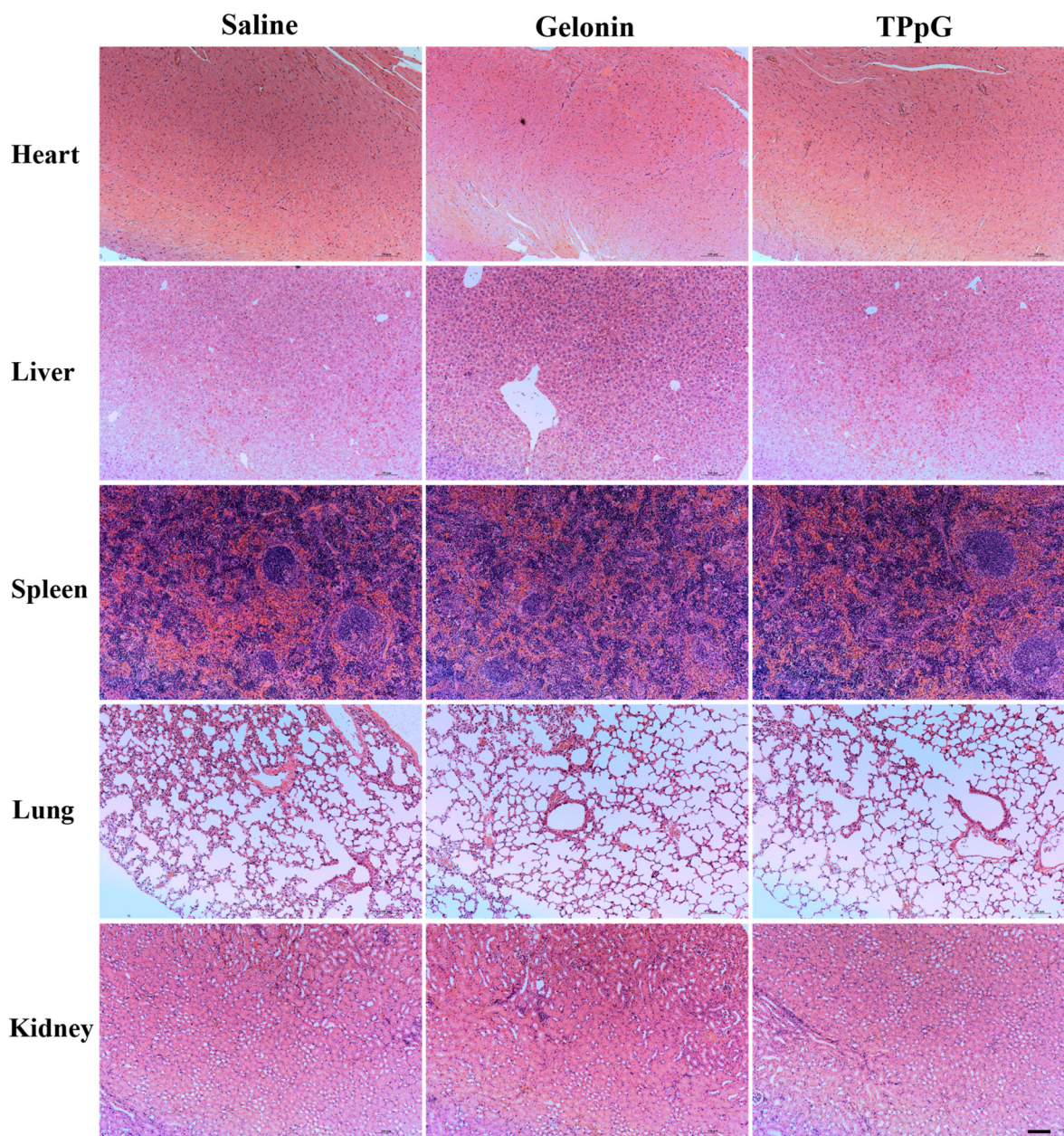
Fig. 8 H&E staining of normal tissues (heart, liver, spleen, lungs and kidneys) of HT1080 tumor-bearing nude mice following different treatments. The scale bar is 100 μm.

To investigate the potential mechanism underlying the anti-cancer activity of TPpG *in vivo*, further histological analysis was conducted in tumor tissues, including immunohisto-chemical analysis of Ki-67 for determining tumor cell proliferation, immunohistochemical staining of caspase-3 and terminal deoxynucleotidyl transferase-mediated dUTP nick-end labeling (TUNEL) assay to evaluate apoptosis. Tumor tissues in the saline group showed the highest expression of Ki-67 and the lowest expression of caspase-3, and no green fluorescence was observed (Fig. 7b). In contrast, gelonin and TPpG treatments suppressed tumor cell proliferation and induced apoptosis to varying degrees. Ki-67 was downregulated, caspase-3 was upregulated and green fluorescence was observed (Fig. 7b). Not unexpectedly, there were the fewest Ki-67 positive proliferating cells and much more caspase-3 positive apoptotic cells in the TPpG-treated tumor tissues, and the strongest green fluorescence was detected (Fig. 7b), supporting the most potent therapeutic effect of TPpG.

To evaluate the *in vivo* biosafety of TPpG, body weights were recorded during the treatment period and the normal tissues (heart, liver, spleen, lungs and kidneys) in each group were excised on day 20 and subjected to H&E staining. As displayed in Fig. 7c, the body weights of BALB/c mice in all groups showed no abnormal change during the 20 days treatment, and the relative body weights fluctuated in the range of 0.99–1.06. Moreover, H&E staining of normal tissues demonstrated that there was no obvious evidence of injury in heart, liver, spleen, lungs and kidneys of mice receiving gelonin or TPpG, and no noticeable cell damage or morphological changes were observed compared to the saline group (Fig. 8). Taken collectively, these results demonstrate that TPpG could efficiently retard subcutaneous HT1080 tumor growth *via* suppressing cell proliferation and triggering cell apoptosis and display favorable systemic safety profiles.

4. Conclusion

This study proposed and successfully biosynthesized a tumor acidity and MMP dual-responsive recombinant plant toxin gelonin, termed TPpG. TPpG comprised four different fragments with distinct functions—Trx, PVGLIG, pHLIP and gelonin. Trx could enhance the solubility and stability of TPpG, PVGLIG and pHLIP endow TPpG with the MMP/pH dual-responsive property, and gelonin exerts antitumor activity *via* inhibiting protein synthesis. TPpG exhibited good thermal and serum stabilities and could enter into MMP2-overexpressing HT1080 cells with high efficiency under acidic conditions. A series of *in vitro* experiments indicated that TPpG displayed apparently augmented cytotoxicity against HT1080 cells at pH 6.5. Mechanistic studies revealed that TPpG resulted in extensive apoptosis and suppressed intracellular protein synthesis. More importantly, TPpG substantially retarded the HT1080 tumor growth *via* restraining cell proliferation and triggering apoptosis. Meanwhile, TPpG showed satisfactory *in vivo* biocompatibility and biosafety, and no noticeable damage to normal tissues was observed. These findings provide promising perspectives for exploring the tumor microenvironment-responsive delivery strategy to achieve safe and effective cancer therapy.

Author contributions

Ding G.-B. conceived the idea, designed the study, performed some experiments and data analysis, wrote the manuscript and supervised the project; Cao H., Zhu C., and Chen F. performed the experiments and data analysis; Ye J. carried out the *in vivo* experiments; Li B.-C. and Yang P. conducted data analysis and provided valuable suggestions; Stauber R. H. revised the manuscript; and Qiao M. and Li Z. supervised the project. All authors contributed to the general discussion. The manuscript was prepared by Ding G.-B. with support from Cao H. and obtained feedback from all co-authors.

Conflicts of interest

The authors declare no competing financial interest.

Acknowledgements

References

1 S. Yao, Z. Wang and L. Li, *Smart Mater. Med.*, 2022, **3**, 230–242.

2 N. Chen, Y. Wang, Y. Zeng, Y. Li, Z. Pan, H. Li, J. Chen, Z. Chen, J. Yuan, W. Yan, Y. J. Lu, X. Liu, Y. He and K. Zhang, *Biomater. Sci.*, 2023, **11**, 828–839.

3 Y. Li, Y. Jiang, Z. Zheng, N. Du, S. Guan, W. Guo, X. Tang, J. Cui, L. Zhang, K. Liu, Q. Yu and Z. Gan, *Adv. Mater.*, 2022, **34**, 2110490.

4 G. Ding, J. Sun, P. Yang, B. Li, Y. Gao and Z. Li, *Mol. Pharmaceutics*, 2018, **15**, 238–246.

5 W. Shen, Y. Zhang, P. Wan, L. An, P. Zhang, C. Xiao and X. Chen, *Adv. Mater.*, 2020, **32**, 2001108.

6 M. C. Shin, J. Zhang, A. E. David, W. E. Trommer, Y. M. Kwon, K. A. Min, J. H. Kim and V. C. Yang, *J. Controlled Release*, 2013, **172**, 169–178.

7 N. Dammes and D. Peer, *Trends Pharmacol. Sci.*, 2020, **41**, 755–775.

8 Q. Guo and C. Jiang, *Acta Pharm. Sin. B*, 2020, **10**, 979–986.

9 X. Liu, F. Wu, Y. Ji and L. Yin, *Bioconjugate Chem.*, 2019, **30**, 305–324.

10 J. Lv, Q. Fan, H. Wang and Y. Cheng, *Biomaterials*, 2019, **218**, 119358.

11 W. Huang, S. Zhou, B. Tang, H. Xu, X. Wu, N. Li, X. Zan and W. Geng, *Acta Biomater.*, 2021, **129**, 199–208.

12 R. Zaman, R. A. Islam, N. Ibnat, I. Othman, A. Zaini, C. Y. Lee and E. H. Chowdhury, *J. Controlled Release*, 2019, **301**, 176–189.

13 V. Graceffa, *Biochimie*, 2023, **213**, 82–99.

14 A. M. Asrorov, Z. Gu, K. A. Min, M. C. Shin and Y. Huang, *ACS Pharmacol. Transl. Sci.*, 2020, **3**, 107–118.

15 Y. Chen, M. Zhang, K. A. Min, H. Wang, M. C. Shin, F. Li, V. C. Yang and Y. Huang, *Curr. Drug Targets*, 2018, **19**, 380–392.

16 B. Li, J. Wei, C. Di, Z. Lu, F. Qi, Y. Zhang, W. S. Leong, L. Li, G. Nie and S. Li, *Acta Pharm. Sin. B*, 2021, **11**, 2059–2069.

17 Z. Setayesh-Mehr and M. Poorsargol, *Mol. Biol. Rep.*, 2021, **48**, 3827–3840.

18 J. Q. Lu, Z. N. Zhu, Y. T. Zheng and P. C. Shaw, *Toxins*, 2020, **12**, 167.

19 G. B. Ding, G. Wu, B. Li, P. Yang and Z. Li, *3 Biotech*, 2019, **9**, 19.

20 Y. Bai, M. Gou, T. Yi, L. Yang, L. Liu, X. Lin, D. Su, Y. Wei and X. Zhao, *Int. J. Med. Sci.*, 2015, **12**, 397–406.

21 T. Mahmood, A. Shahbaz, N. Hussain, R. Ali, H. Bashir and K. Rizwan, *Int. J. Biol. Macromol.*, 2023, **230**, 123161.

22 M. C. Shin, J. Zhang, K. A. Min, K. Lee, C. Moon, J. P. Balthasar and V. C. Yang, *J. Controlled Release*, 2014, **194**, 197–210.

23 M. C. Shin, J. Zhao, J. Zhang, Y. Huang, H. He, M. Wang, K. A. Min and V. C. Yang, *J. Biomed. Mater. Res., Part A*, 2015, **103**, 409–419.

24 M. C. Shin, J. Zhang, K. A. Min, H. He, A. E. David, Y. Huang and V. C. Yang, *Pharm. Res.*, 2015, **32**, 2690–2703.

25 M. C. Shin, K. A. Min, H. Cheong, C. Moon, Y. Huang, H. He and V. C. Yang, *Pharm. Res.*, 2016, **33**, 2218–2228.

26 S. H. Ham, K. A. Min and M. C. Shin, *Acta Pharmacol. Sin.*, 2017, **38**, 897–906.

27 S. Ham, K. A. Min, J. W. Yang and M. C. Shin, *Arch. Pharmacal Res.*, 2017, **40**, 1094–1104.

28 T. Park, K. A. Min, H. Cheong, C. Moon and M. C. Shin, *J. Drug Targeting*, 2019, **27**, 950–958.

29 M. G. Vander Heiden, L. C. Cantley and C. B. Thompson, *Science*, 2009, **324**, 1029–1033.

30 X. Wang, X. Wang, S. Jin, N. Muhammad and Z. Guo, *Chem. Rev.*, 2019, **119**, 1138–1192.

31 A. A. Svoronos and D. M. Engelman, *Proc. Natl. Acad. Sci. U. S. A.*, 2021, **118**, e2016605118.

32 N. U. Dharmaratne, A. R. Kaplan and P. M. Glazer, *Cells*, 2021, **10**, 541.

33 H. Han, Y. Hou, X. Chen, P. Zhang, M. Kang, Q. Jin, J. Ji and M. Gao, *J. Am. Chem. Soc.*, 2020, **142**, 4944–4954.

34 A. M. Demin, A. G. Pershina, A. S. Minin, O. Y. Brikunova, A. M. Murzakaev, N. A. Perekucha, A. V. Romashchenko, O. B. Shevelev, M. A. Uimin, I. V. Byzov, D. Malkeyeva, E. Kiseleva, L. V. Efimova, S. V. Vtorushin, L. M. Ogorodova and V. P. Krasnov, *ACS Appl. Mater. Interfaces*, 2021, **13**, 36800–36815.

35 A. Moshnikova, M. DuPont, H. Visca, D. M. Engelman, O. A. Andreev and Y. K. Reshetnyak, *Front. Oncol.*, 2022, **13**, 1023959.

36 C. J. Cheng, R. Bahal, I. A. Babar, Z. Pincus, F. Barrera, C. Liu, A. Svoronos, D. T. Braddock, P. M. Glazer, D. M. Engelman, W. M. Saltzman and F. J. Slack, *Nature*, 2015, **508**, 107–110.

37 M. Sahraei, B. Chaube, Y. Liu, J. Sun, A. Kaplan, N. L. Price, W. Ding, S. Oyaghire, R. García-Milian, S. Mehta, Y. K. Reshetnyak, R. Bahal, P. Fiorina, P. M. Glazer, D. L. Rimm, C. Fernández-Hernando and Y. Suárez, *J. Clin. Invest.*, 2019, **129**, 5518–5536.

38 A. R. Kaplan, H. Pham, Y. Liu, S. Oyaghire, R. Bahal, D. M. Engelman and P. M. Glazer, *Mol. Cancer Res.*, 2020, **18**, 873–882.

39 A. Y. Frolova, A. A. Pakhomov, D. L. Kakuev, A. S. Sungurova, S. M. Deyev and V. I. Martynov, *Biochem. Biophys. Res. Commun.*, 2022, **612**, 141–146.

40 T. Chu, B. Cao, P. Wang, B. Li, J. Ren, G. Nie, J. Wei and S. Li, *Bioconjugate Chem.*, 2023, **34**, 1894–1901.

41 Z. Zong, X. Liu, Z. Ye and D. Liu, *Proc. Natl. Acad. Sci. U. S. A.*, 2023, **120**, e2214912120.

42 G. B. Ding, J. Sun, G. Wu, B. Li, P. Yang, Z. Li and G. Nie, *ACS Appl. Mater. Interfaces*, 2018, **10**, 5227–5239.

43 G. B. Ding, C. Zhu, Q. Wang, H. Cao, B. C. Li, P. Yang, R. H. Stauber, G. Nie and Z. Li, *Bioact. Mater.*, 2022, **18**, 42–55.

44 G. B. Ding, X. Ma, X. Meng, P. Yang, R. H. Stauber and Z. Li, *Mater. Des.*, 2021, **212**, 110197.

45 M. Li, T. Yan, Y. Cai, Y. Wei and Q. Xie, *Gene*, 2023, **850**, 146927.

46 Q. Yao, L. Kou, Y. Tu and L. Zhu, *Trends Pharmacol. Sci.*, 2018, **39**, 766–781.

47 W. Gao, B. Xiang, T. T. Meng, F. Liu and X. R. Qi, *Biomaterials*, 2013, **34**, 4137–4149.

48 P. Ramezania, K. Abnous, S. M. Taghdisi, M. Zahiria, M. Ramezani and M. Alibolandi, *Colloids Surf., B*, 2020, **193**, 111135.

49 V. Vichai and K. Kirtikara, *Nat. Protoc.*, 2006, **1**, 1112–1116.

50 K. Cheng, Y. Ding, Y. Zhao, S. Ye, X. Zhao, Y. Zhang, T. Ji, H. Wu, B. Wang, G. J. Anderson, L. Ren and G. Nie, *Nano Lett.*, 2018, **18**, 3250–3258.

51 E. R. LaVallie, E. A. DiBlasio-Smith, L. A. Collins-Racie, Z. Lu and J. M. McCoy, *Methods Mol. Biol.*, 2003, **205**, 119–140.

52 J. Schuster, H. C. Mahler, S. Joerg, J. Huwyler and R. Mathaes, *J. Pharm. Sci.*, 2021, **110**, 3103–3110.

53 R. Goswami, T. Jeon, H. Nagaraj, S. Zhai and V. M. Rotello, *Trends Pharmacol. Sci.*, 2020, **41**, 743–754.

54 G. Salzano, D. F. Costa, C. Sarisozen, E. Luther, G. Mattheolabakis, P. P. Dhargalkar and V. P. Torchilin, *Small*, 2016, **12**, 4837–4848.

55 B. J. C. Quah, H. S. Warren and C. R. Parish, *Nat. Protoc.*, 2007, **2**, 2049–2056.